CHEMISTRY OF MATERIALS
Article

Chem. Mater. **2009,** *21,* 5637–5643 5637
DOI:10.1021/cm900845h

Development of Hexagonal Closed-Packed Cobalt Nanoparticles Stable at High Temperature

Víctor A. de la Peña O′Shea,*[,†,‡] Pilar Ramírez de la Piscina,[‡] Narcis Homs,[‡] Guillem Aromí,[‡] and José L. G. Fierro[§]

[†]*Instituto Madrileño de Estudios Avanzados en ENERGIA, C/Tulipan s/n 28933, Móstoles, Madrid, Spain,* [‡]*Departament de Química Inorgànica and Institut de Nanociència i Nanotecnologia, Univesitat de Barcelona, 08028 Barcelona, Spain, and* [§]*Instituto de Catálisis y Petroleoquímica, CSIC, C/ Marie Curie s/n, Cantoblanco, 28049 Madrid, Spain*

Received March 26, 2009. Revised Manuscript Received August 29, 2009

Cobalt metal particles have several stable phases depending on their size and the temperature employed in the preparation. The face-centred cubic (fcc) structure is thermodynamically stable above 450 °C, whereas the hexagonal-closed packed (hcp) phase is stable at lower temperatures. Cobalt oxide reduction carried out under H_2 atmosphere leads to fcc-Co phase. This study shows that the reduction of cobalt oxide under CO or H_2+CO mixtures giver rise to the formation of a hcp-Co phase, which still remains stable at high temperatures (up to 700°C). This circumstance is due to the encapsulation of hexagonal cobalt nanoparticles by carbon nanofibers that minimizes the surface energy of these cobalt structures. Moreover, this encapsulation effect prevents the sintering and oxidation reactions of hcp-Co metallic phase even at a high temperature (up to 700°C) Thus, the reduction atmosphere plays a key role in the formation and stabilization of these cobalt phases.

Introduction

Transition metal nanoparticles are being extensively investigated with great interest from both academic and industrial sides. Thanks to their chemical, magnetic, electronic, and optical properties, they are used in a wide range of applications, such as magnetic data storage,[1a] solar energy conversion,[1b] sensors,[1c] solid electrolytes,[1c] bioengineering applications[1e] and catalysis.[1f,g] A good control of the size, shape, composition, and thermal stability of the metal nanoparticles is vital for controlling their properties. To do so, it is necessary to optimize the variables that control nanoparticle synthesis.

Cobalt nanoparticles are good candidates to obtain catalytic materials or magnetic self-assembled structures with potential applications in catalysis[1f,g] and information storage,[1a] among others. In recent years, several groups have concentrated their efforts on the preparation and characterization of these systems.[2] These metallic cobalt nanoparticles have three different crystal structures: hexagonal closed-packed (hcp) (α), face-centered cubic (fcc) (β), and primitive cubic phase (ε),[2a,b] which possess similar energetic stabilities but different properties, as shown in recent theoretical studies.[3a] These three structures possess interesting magnetic properties because of the room-temperature anisotropy of the ε,[3b] fcc,[3c] and hcp[3d] phases. The hcp phase possesses the higher anisotropy and is a preferred material for magnetic recording applications. DFT calculations carrying out by our group show that both shape and crystal phase are critical points in the magnetic behavior of cobalt nanoparticles. Moreover, we observed experimentally that the behavior of cobalt-based supported catalysts in Fischer−Tropsch synthesis depends on the characteristics of the metallic phase (i.e., fcc or hcp),[1g] as confirmed by theoretical studies[3a] showing that the FTS reaction is structure sensitive and that Co-hcp phase presents better results.

Thus, hcp-cobalt nanoparticles have many applications. However, nanocrystalline particles are very sensitive to the temperature and environment; therefore, structure and morphological properties of cobalt phase

*To whom correspondence should be addressed. E-mail: victor.delapenya@imdea.org.

(1) (a) Thompson, D.; Best, J. S. *IBM J. Res. Dev.* **2000**, *44*, 311. (b) O'Regan, B.; Grätzel, M. *Nature* **1991**, *353*, 737. (c) Rolison, D. R. *Chem. Rev.* **1990**, *90*, 867.(d) Murugesamoorthi K. A., Srinivasan S., Appleby A. J. Research, Development and Demonstration of Solid Oxide Fuel Cell Systems. In *Fuel Cell System*; Blomen, L-J. M. J., Mugerwa, M. N., Eds.; Plenum: New York, 1993. (e) Pauser, S.; Reszka, R.; Wagner, S.; Wolf, K. J. *Anti-cancer Drug Des.* **1997**, *12*, 125. (f) Somorjai, G. A.; Borodko, Y. G. *Catal. Lett.* **2001**, 76. (g) de la Peña O′Shea, V. A.; Campos-Martín, J. M.; Fierro, J. L. G. *Catal. Comm.* **2004**, *5*, 635.

(2) (a) Puntes, V. F.; Krishnan, K. M.; Alivisatos, A. P. *Science* **2001**, *291*, 2115. (b) Sun, S.; Murray, C. B. *J. Appl. Phys.* **1999**, *85*, 4325. (c) Skumryev, V.; Stoyanov, S.; Zhang, Y.; Hadipanayis, G.; Givord, D.; Nogues, J. *Nature* **2003**, *423*, 850.

(3) (a) de la Peña O'Shea V.A., Álvarez-Galván M.C., Campos Martín J.M., Gonzalez S., Illas F., Fierro J.L.G. *International Symposium on Catalysis for Clean Energy and Sustainable Chemistry*; Madrid, June 17−20, 2008. (b) Puntes, V. F.; Krishnan, K. M. *IEEE Trans. Mag.* **2001**, *37*, 2210. (c) Yang, H. T.; Shen, C. M.; Su, Y. K.; Yang, T. Z.; Gao, H. J.; Wang, Y. G. *Appl. Phys. Lett.* **2003**, *82*, 4729. (d) Gambardella, P.; Rusponi, S.; Veronese, M.; Dhesi, D. D.; Grazioli, C.; Dallmeyer, A.; Cabria, I.; Zeller, R.; Dederichs, P. H.; Kern, K.; Carbone, C.; Brune, H. *Science* **2003**, *300*, 1130.

Published on Web 11/11/2009

are key factors to be considered. From the point of view of the structural properties, α (hcp) and β (fcc) phases display similar structures, although they differ in the stacking sequence of the [111] plane. Both phases are usually found in a given sample because of the low energy required for stacking fault formation.[4] However, although both phases can coexist at room temperature, the hcp bulk phase is stable below the allotropic transformation temperature 420−450 °C (depending on crystal size), whereas the fcc structure is thermodynamically stable above this temperature.[5] Several studies have been conducted in order to explain and control this transformation,[5c,d] although the origin of this behavior in Co still remains ambiguous in spite of intensive efforts.

Becaues of the special properties of hcp cobalt nanoparticles it is necessary to design new preparation routes giving rise to α-Co phase stable at high temperature. The present communication presents a preparation method to obtain hcp Co nanoparticles stable at high temperature by encapsulating them within carbon fibers. To follow the nanoparticles and carbon coated formation, we carried out an in situ X-ray diffraction analysis and extensive characterization of precursor and formed Co nanoparticles using scanning electron microscopy (SEM), X-ray photoelectron spectroscopy (XPS), high-resolution transmission electron microscopy (HRTEM), and electron energy loss spectroscopy (EELS).

Experimental Section

Synthesis. The cobalt oxide sample (Co_3O_4) was prepared via precipitation adjusting pH at 12 by addition of a NaOH aqueous solution over a $Co(NO_3)_2 \cdot 6H_2O$ aqueous solution. Later on, the precipitate was aged using a reflux system at 80 °C under an air atmosphere. The precipitate was washed with water and was transferred to a hot air oven at 110 °C overnight. Precursor calcination was carried out at 450 °C for 4 h under air atmosphere. Finally, the cobalt oxide sample was reduced under different atmospheres: H_2, CO, and H_2+CO (syngas) by increasing the temperature from 25 to 700 °C (the technique used for these treatments is extensively explained in the experimental section of the Supporting information).

X-ray Powder Diffraction (XRPD) Experiment. X-ray powder diffraction (XRD) measurements were performed using a Bragg-Brentano $\theta/2\theta$ Siemens D-500 diffractometer (radius = 215.5 mm), using nickel-filtered $CuK_{\alpha 1}$ ($\lambda = 0.15406$ nm). The divergence slit was of 1° and the receiving slit of 0.15°. The diagrams were scanned between 20 and 80° Bragg angle, with a step width of 0.02° and counting 5 s at each step. Powder X-ray diffraction study was also carried out under in situ conditions in a Siemens D-500 X-ray diffractometer equipped with an ANTON PAAR chamber in which a reactor-cell (platinum laminate) containing the sample was placed. The diagrams were scanned between 34 and 54° Bragg angle, with a step width of 0.08° and counting 3s at each step. The gas flow (Hydrogen, carbon monoxide, syngas) was introduced with constant flow of 40 mL/min using a Brooks (model 5850TR) mass flow controller. Temperature was measured by a thermocouple in contact with the sample holder. The sample was heated from 25 to 700 °C with a heating rate of 5°C/min. The in situ XRD patterns were measured at constant temperature.

Morphological Study. The morphological structure of the samples was revealed by scanning electron microscopy (SEM) in a field-emission SEM (FE-SEM) Hitachi H-4100FE operated with intensity current between 15 and 20 kV and current of 10 mA (1.5 nm resolution). Powder samples were pressed and mounted on a sample rod. The fresh and H_2 reduced samples were coated with a thin graphite layer to prevent the accumulation of static charge derived from the electron beam.

Surface Analysis. XPS Surface analysis was carried out on a SAGE-SPECS spectrometer equipped with a hemispherical electron analyser and a Mg Kα ($h\nu = 1253$ eV) 125 W X-ray source. The powder samples were pressed and then mounted on C conductive tabs. The base pressure in the analysis chamber was maintained below 4×10^{-9} mbar during data acquisition. The area under analysis was around 2.4 mm^2 and the pass energy of the analyser was set at 50 eV, for which the resolution as measured by the full width at half maximum (FWHM) of the $Au4f_{7/2}$ core level was 1.7 eV. The binding energies were referenced to the C1s peak at 284.9 eV due to adventitious carbon. Data processing was performed with the Casa XPS program package. The spectra were decomposed with the least-squares fitting routine provided with the software using pseudo-Voight function and after subtracting a Shirley background. Atomic fractions were calculated using peak areas normalized on the basis of sensitivity factors.

Transmission Electron Microscopy. Cobalt samples treated with H_2+CO at 700°C were also analyzed by high-resolution transmission electron microscopy (HRTEM) with the aim of determining the form, shape, and distribution of both cobalt particles and carbon nanofibers. Moreover, a spectroscopy study by electron energy loss spectroscopy (EELS) was also performed. Thus, two kinds of HRTEM equipment were used to carried out these studies: A) For HRTEM analysis a Philips CM-30 electron microscope equipped with a LaB_6 source and operated at 300 kV, with a 0.19-nm point resolution. Magnification and camera constants were calibrated using appropriate standards under the same electron-optical conditions. For data treatment, Fourier-transformed images were obtained by using local software on digitized parts of the negatives. (B) High-resolution transmission electron microscopy and electron energy loss spectroscopy were performed with a JEOL JEM 2010F instrument working at 200 kV and equipped with a field emission source, equipped with a Gatan imaging filter (GIF) and an Oxford X-ray energy dispersive spectroscopy (EDS) system. Elemental mapping was performed with the GIF using the three windows technique. The maps of the different elements were obtained using the $CoL_{2,3}$ edge at 779 eV, C K-edge at 284 eV, O K-edge at 583 eV. Samples for both HRTEM studies were prepared by putting an aliquot of ethanol solution with a suspension of nanocrystals onto an amorphous carbon substrate supported on a copper grid. The excess liquid was removed and the grid was dried at room temperature. The image reconstruction was realized from Fourier transforms image, by means of inverse Fourier transform tools provided by the Transform DigitalMicrograph (M) v 3.7.0 package.

Magnetic Properties. Variable-temperature magnetic measurements were carried out on polycrystalline samples using a

(4) Dinega, D. P.; Bawendi, M. G. *Angew. Chem., Int. Ed.* **1999**, *38*, 1788.
(5) (a) Zhao, Z. Q.; Veintemillas-Verdaguer, S.; Bormati-Miguel, O.; Morales, M. P.; Xu, H. B. *Phys. Rev. B* **2005**, *71*, 24106.. (b) Puntes, V. F.; Zanchet, D.; Erdonmez, C. K.; Alivisatos, A. P. *J. Am. Chem. Soc.* **2002**, *124*, 12874. (c) Sato, H.; Kitakami, O.; Sakurai, T.; Shimada, Y.; Otani, Y.; Fukamichi, K. *J. Appl. Phys.* **1997**, *81*, 1858. (d) Kitakimi, O.; Sato, H.; Shimada, Y.; Sato, F.; Tanaka, M.. *Phys. Rev. B* **1997**, *56*, 13849.

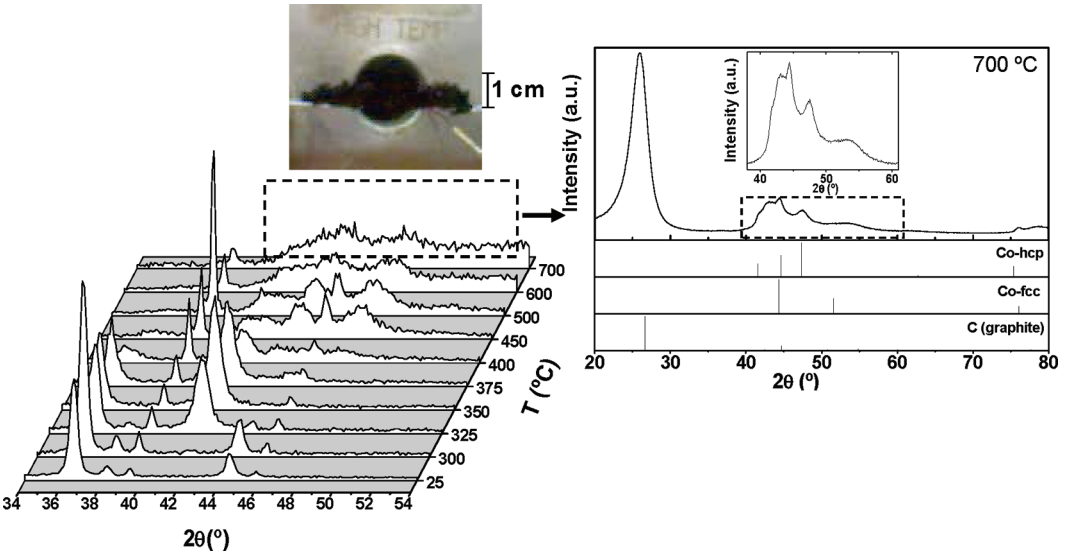

Figure 1. In situ X-ray diffraction patterns of the Co_3O_4 sample treated with H_2+CO mixture, as a function of temperature. Peaks at 39.6 and 46.1° are due to the platinum holder (left). X-ray diffraction profiles of sample at 700 °C (right) and selected area diffraction profile of metallic cobalt (inset). The picture of the sample after reduction treatment shows hcp cobalt nanoparticles encapsulating in carbon nanofibers formed in the X-ray sample holder (top).

Quantum Design MPMS XL-5 SQUID susceptometer operating at a variable magnetic field and at temperatures of 5 and 300 K.

Results and Discussion

To study the effect of the reduction treatment and to monitor the crystal phase formation of cobalt nanoparticles, we performed several in situ XRD experiments. Figure 1 shows the in situ XRD profiles of Co_3O_4 treated in a H_2+CO atmosphere from 25 to 700 °C.

At 25 °C, peaks are detected only at 36.7, 38.4, and 44.7°, corresponding to (311), (222), and (400) reflections of the initial Co_3O_4 sample with a spinel structure. These peaks progressively disappear upon increasing temperature, whereas new ones corresponding to CoO phase (36.3° (111), 42.3° (200)) appear. When the temperature is increased to 400 °C, the intensity of CoO diffraction peaks diminishes and a broad peak appears, although it does not belong to a cobalt phase. At 450 °C, the diffraction pattern displays three peaks centered at 41.7° (100), 44.5° (002), and 47.5° (101), which can be ascribed to the hcp-Co phase. However, at this temperature, a fraction of the CoO phase still remains unreduced. A further temperature increase leads to its progressive disappearance. When temperature reaches 600 °C, the XRD profile starts to lose the characteristic diffraction peaks and at 700 °C almost all diffraction lines disappear. This result is related to carbon formation. The growth of these carbon phases over the sample holder (Figure 1, top) is responsible for the loss of diffraction planes.

Further insight on the reduction processes can be obtained by ex situ XRD experiments of several samples after reduction treatment in an H_2+CO atmosphere at different temperatures. Figure 1 (right) shows the XRD profile of Co_3O_4 reduced in (H_2+CO) atmosphere at 700 °C. The large amount of carbon nanostructures generated at 700 °C makes difficult the assignment of characteristic diffraction lines. Accordingly, ex situ XRD profiles recorded at 600 °C were analyzed in major detail (see Figure 2). The diffraction pattern depicts the presence of a major hcp-Co phase with a minor fcc-Co phase, as confirmed by the low intensity of the diffraction peak centred at 51.2° (111) that is characteristic of this cubic phase. The very low presence of fcc-cobalt phase is principally due to the cobalt not covered by carbon nanofibers; besides, the hydrogen present in the treatment could hydrogenate the nanofibers top given the phase change from hcp to fcc because of the high temperature. The presence of a Co_2C phase cannot be ruled out because of the appearance of the characteristic diffraction peaks (56.7°). Nevertheless, some of this characteristic diffraction line of the carbide phase coincides with that of the unreduced CoO phase. Moreover, this phase could be present in the cobalt carbon interface. In addition, a major broad peak is observed at 25.8°, which corresponds to the plane (002) of a carbon nanostructure with an interlayer spacing of 0.345 nm. This value is slightly larger than the single-crystal graphite value (0.335 nm). Several authors have studied the variation in this lattice spacing[6] and proposed that the intershell spacing decreases asymptotically with increasing tube diameter. The interlayer spacing value and tube diameter average ($\approx$ 22 nm), which is in agreement with that reported by Kiang et al.[6c]

On the other hand, in situ XRD patterns of samples reduced under CO atmosphere up to 700 °C (Figure S1, Supporting Information) show that Co_3O_4 starts to be transformed to CoO at 325 °C. At 450 °C, a low-intensity diffraction line centered at ca. 44.1°, indicative of the formation of metallic cobalt, is observed. Upon increasing reduction temperature up to 475 °C under a CO

(6) (a) Ijima, S. *Nature* **1991**, *354*, 56. (b) Sun, X.; Kiang, C. H.; Endo, M.; Takeuchi, K.; Furuta, T.; Dresselhaus, M. S. *Phys. Rev. B* **1996**, *54*, 1269. (c) Kiang, C. H.; Endo, M.; Majayan, P.; Dresselhaus, G.; Dresselhaus, M. S. *Phys. Rev. Lett.* **1998**, *81*, 1869.

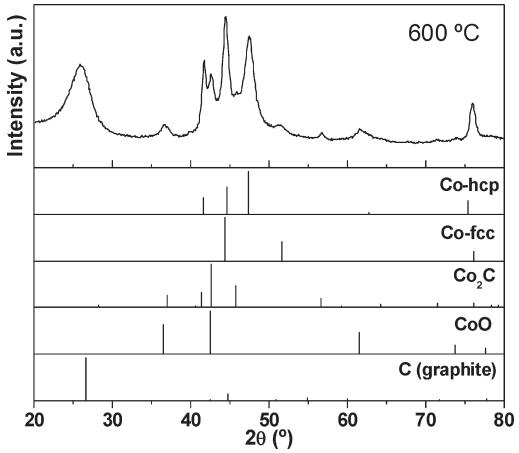

Figure 2. X-ray diffraction profiles and diffraction patterns of sample after H_2+CO treatment at 600 °C.

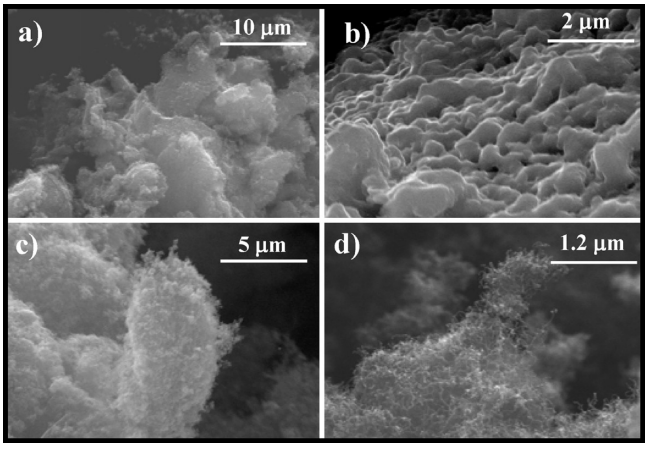

Figure 3. SEM image of: (a) Co_3O_4 fresh sample, and after different reduction treatments at 700 °C, (b) H_2, (c) CO, and (d) H_2+CO.

atmosphere, crystalline phases of Co^0 are developed. The diffraction peaks at 42.1, 44.2, 47.2, and 51.3° point to the presence of both fcc-Co and hcp-Co. These cobalt phases are present until 700 °C, although the proportion of the fcc-Co phase is higher as compared to that obtained under H_2+CO treatment. Thus, with the treatment of cobalt precursor under a CO atmosphere, two types of reduction process take place: (i), the reduction of Co_3O_4 precursor to CoO and Co^0 (see afterwards); and (ii), carbon deposition on the metallic cobalt particles via the Boudouard CO disproportionation reaction[7]

$$2CO(g) \rightarrow CO_2(g) + C\downarrow(s) \qquad (1)$$

This reaction gives rise to the formation of both amorphous and nanostructured carbon deposits. The growth mechanism of the carbon nanostructures[8] assumes that molecular CO decomposition and carbon solution occur on one side of the metal particle. In addition, both the metal particle and the carbon nanostructures are formed simultaneously. The smaller particles display a high proportion of exposed atoms, thus developing a high surface energy per atom. This surface energy decreases when the carbon binds to the cobalt particles. When the metal particle becomes supersaturated, the carbon atoms start to diffuse through the particle and precipitate on the opposite side of the particle, leading to the formation of carbon nanostructures. The carbon diffusion is limited by domain size within the metal particle.

Previous studies[9] showed that different carbon structures are developed depending on the preparation conditions. Thus, carbon nanotubes (CNT) and carbon nanofibers (CNF) can be obtained. Pinheiro et al.[9a] reported that the carbon deposits originating from CO disproportionation are composed mainly of nanotubes. By contrast, if H_2 is added to CO, only nanofibers are developed. This observation suggests that the hydrogen atoms satisfy the valence at the edge of each graphite basal plane. Moreover, as a consequence of the hydrogen effect, the rate of carbon deposition and its total amount is increased, yet the most noticeable effect is the change in carbon morphology. Thus, adding H_2 to the CO feed results in the formation of carbon layers inclined with respect to the tube axis and exhibit a "herringbone structure", as evidenced by stacking of cone-segment carbon layers.

Finally, with the aim of studying the hydrogen effect, in situ XRD patterns of Co_3O_4 was performed under a H_2 atmosphere at different temperatures (Figure S2, Supporting information). The Co_3O_4 precursor starts to be reduced at 325 °C. At this temperature, two main diffraction lines located at 36.3 and 42.2°, assigned to CoO (111) and CoO (100) planes, are observed. A further increase in temperature up to 350 °C gives rise to partial reduction of CoO to metallic cobalt as evidenced by the appearance of new peaks at 44.1 and 51.2° belonging to fcc-Co (111) and fcc-Co (200) diffraction planes, respectively. Upon increasing reduction temperature up to 700 °C, only the diffraction peaks of fcc-Co are observed, but in no case do lines belonging to the hcp-Co phase appear. During the reduction process under H_2 atmospheres, Co_3O_4 is reduced to metallic cobalt in two stages

$$Co_3O_4(s) + H_2(g) \rightarrow 3CoO(s) + H_2O(g) \qquad (2)$$

$$CoO(s) + H_2(g) \rightarrow Co^0(s) + H_2O(g) \qquad (3)$$

The morphological changes brought about by the reduction treatments of the samples were monitored by scanning electron microscopy (SEM). The SEM image in Figure 3a of the fresh Co_3O_4 sample shows particles with different size and shape. The SEM image of the Co_3O_4 sample reduced at 700 °C (Figure 3b) exhibits a "flake" morphology as a consequence of the sintering of Co^0 particles generated during reduction process. Images c

(7) (a) Guerret-Plecourt, C.; Bouar, Y. L.; Loseau, A.; Pascard, H. *Nature* **1994**, *372*, 761. (b) Liu, S.; Zhu, J.; Mastai, Y.; Felner, I.; Gedanken, A. *Chem. Mater.* **2000**, *12*, 2205.
(8) Boskovic, B. J.; Stolojan, V.; Khan, R. U. A.; Haq, S.; Silva, R. P. *Nat. Mater.* **2002**, *1*, 165.
(9) (a) Pinheiro, J. P.; Schouler, M. C.; Doryhee, E. *Solid State Commun.* **2002**, *123*, 161. (b) Pinheiro, J. P.; Schouler, M. C.; Gadelle, P.; Mermoux, M..; Dooryhee, E. *Carbon* **2000**, *38*, 1469. (c) Jiao, J.; Seraphin, S. *J. Phys. Chem. Solids* **2000**, *61*, 1055. (d) Herreyre, S.; Gadelle, P. *Carbon* **1995**, *33*, 24.

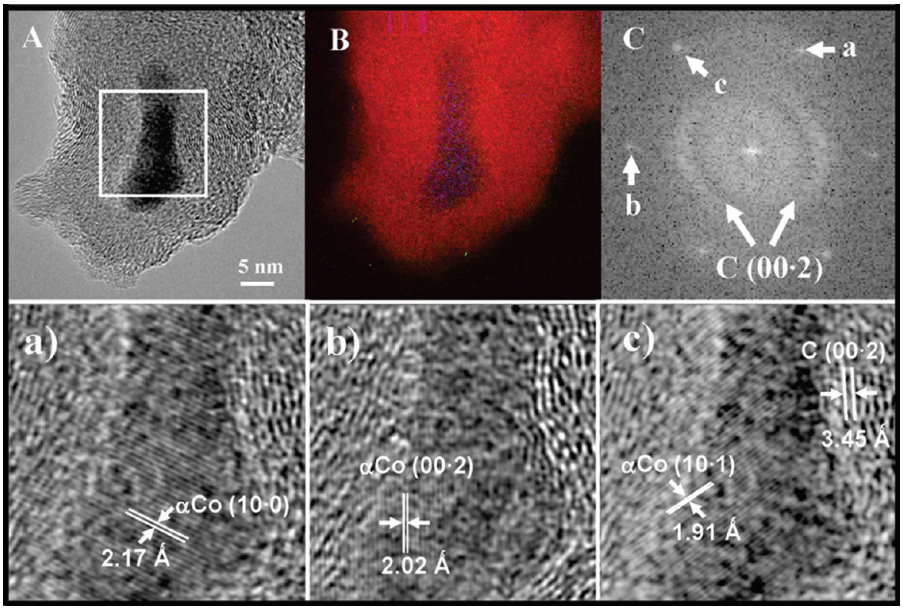

Figure 4. (A) High-resolution TEM imaging (carbon nanofibers filled with an hcp-Co nanoparticle) of Co_3O_4 reduced in an H_2-CO atmosphere at 700 °C, with the square marking the area studied. (B) Specific oxygen K-edge energy loss image (green), carbon K-edge (red) and Co L-edge (blue). (C) Fourier Transform images of the selected area. The bottom of the figure shows the reconstructed images corresponding to the different spots: (a) α-Co (10·0) plane (2.17 Å), (b) α-Co (00·2) plane (2.02 Å), and (c) α-Co (10·1) plane (1.91 Å).

and d in Figure 3 show the SEM images of Co_3O_4 sample reduced under CO and H_2+CO atmospheres at 700 °C, respectively. These images clearly show that carbon nanostructures grew on the cobalt particles acting as support. It can also be seen that the (H_2+CO) treatment gives rise to a larger population of these structures. In addition, the length and diameter of the carbon nanostructures obtained under H_2+CO treatment are higher than with CO treatment (see Figure S3 in the Supporting Information).

Photoelectron spectra of the Co_3O_4 samples treated in H_2+CO mixture at different temperatures (500 °C (A) and 700 °C (B)) were recorded. The convoluted C1s spectrum for both samples shows the peak characteristic of the C sp^2 orbital,[10] and a second contribution due to the binding energy characteristic of C sp^3 hybridized carbon species in carbon nanostructure materials (see Table 1, XPS section, in the Supporting Information). The appearance of this contribution could be explained by hybridization from sp^2 to sp^3 because of C−H bond formation.[10b] The percentage of carbon contributions in the sample surface shows a minor percentage of hydrogenated carbon atoms for the sample treated at 700° C, because the C−H bonds formed are stable at temperatures below 600 °C.[10b] The C/Co ratio calculated from XPS for the samples A (500 °C) and B (700 °C) were 5.7 and 16.1, respectively. The higher value observed for sample B indicates that CNF formation increases at high temperature and most of the cobalt became covered by carbon.

The transmission electron microscopy (TEM) images of the Co_3O_4 sample treated in H_2+CO at 700 °C revealed the formation of large amounts of carbon nanostructures of slightly different diameters, originated from cobalt particles that are encapsulated at the top of the nanostructure (see Figure S4 in the Supporting Information). Thus, TEM images reveal the presence of the fishbone-type CNF with the typical hollow nature of this kind of material.

High-resolution TEM analysis after different treatments allows an accurate characterization of cobalt nanoparticles. Figure 4 shows a high resolution image of the Co_3O_4 sample after H_2+CO treatment at 700 °C (A) along with the map of selected elements Co, C, and O (B), and the Fourier Transform (FT) images (C) of selected areas (labeled as a, b, and c). Figure 4A depicts an individual cobalt particle of about 5 nm (width) and 20 nm (height), encapsulated in the CNF. The mapping shown in Figure 4B reveals complete coverage of the cobalt particle by the CNF and the absence of oxygen. Moreover, this image shows the graphene layers lying in parallel to the surface of the cobalt particle in a stacked-up structure. The FT image of the selected area, as shown in Figure 4C, exhibits strings in various crystallographic directions (a, b, and c in the figure) along the CNF halo with a lattice fringe of 3.45 Å. The bottom of Figure 4 shows the reconstructed images corresponding to the different planes and lattice fringes of (a) Co (10·0) plane (2.17 Å); (b) Co (00·2) plane (2.02 Å); and (c) Co (10·1) plane (1.91 Å), corresponding to a hexagonal metallic cobalt phase. All individual metallic particles analyzed by HRTEM in the catalyst record similar results (see also Figure S5 in the Supporting information). The EELS spectrum shows the simultaneous presence of cobalt and carbon, with an approximate C:Co atomic ratio of 17.8:1 (see Figure S6 in the Supporting Information). These data agree with the results obtained by XPS (see above).

(10) (a) Okapulugo, T. I. T.; Papakonstantinou, P.; Murphy, H.; McLaughlin, J.; Brown, N. M. D. *Carbon* **2005**, 43,153. (b) Nikitin, A.; Ogasawara, H.; Mann, D.; Denecke, R.; Zhang, Z.; Dai, H.; Cho, K.; Nilson, A. *Phys. Rev. Lett.* **2005**, *95*, 22507.

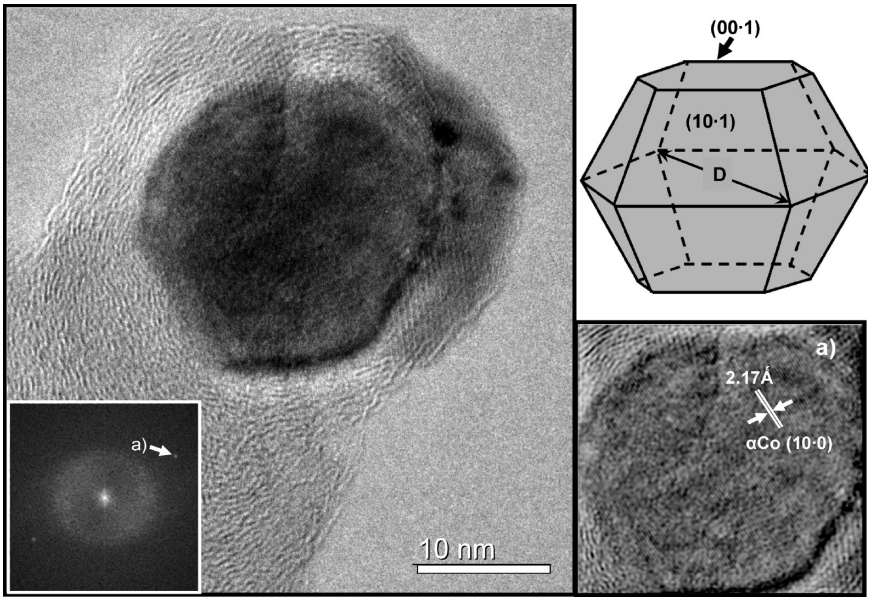

Figure 5. High-resolution TEM image of a hexagonal shaped Co particle of $D \approx 20$ nm encapsulated in a CNF. The particle shows the lattice fringe ($d =$ 2.17 Å) from the plane (10·0) of highly crystalline α-Co. The inset shows the Fourier Transform of the image depicting the α-Co (10·0) plane. (a) reconstructed images corresponding to this lattice fringe; the Wulff polyhedron of α-Co constructed by the Gibbs−Wulff relation[11] is also shown (right top).

High-resolution TEM analysis revealed two types of shapes for the hcp-Co particles: polyhedral and irregular. It is noticeable that several particles display well-defined crystal habits and some of them are single crystals. Figure 5 shows a high-resolution TEM image with an example of a particle whose shape could be consistent with the Wulff polyhedron of hcp-Co.[5d] This Wulff polyhedron follows the Gibbs-Wulff relation[11]

$$\sum \gamma_i S_i = \text{minimum}$$

where γ_i is the surface free energy of the ith crystal face whose surface area is S_i.

Moreover, the FT image of the selected area shown in Figure 5 (inset) exhibits one string in only one crystallographic direction. The analysis of the reconstructed images, corresponding to this string, shows a lattice fringe of 2.17 Å corresponding to the (10·0) plane of hcp-Co.

Thus, the results obtained by TEM analysis show a hcp-cobalt nanoparticle whose shape is consistent with a α-Wulff polyhedron and other slightly distorted with a mean diameter of $d \geq 20$ nm (3D cobalt particle, Wulff polyhedron, is also shown in the figure). These results are in agreement with the studies carried out by Kitami et al.[5b] who conducted an exhaustive study of the particle size effect on crystal phase and the stability of Co particles. They calculated the total free energies as a function of crystal size for several Wulff polyhedrons found in the cobalt crystal phases and conclude that α-Wulff polyhedron is stable in particles with $d \geq$ 20 nm.

From the structural point of view, the stability of the cobalt phase is governed by the contribution of surface energy to the system's overall energy. One of the factors affecting the phase transformation of Co nanoparticles is the change in surface energy. The surface energy of hcp-Co particles is around 14% higher than for fcc-Co; therefore, the hcp-Co becomes destabilized simply for reasons of surface energy.[12] This higher surface energy is due to the considerable differences in the dimensions of the unit cell of the hexagonal and fcc-Co phases. Thus, small particles are subjected to higher surface force than large particles, due to surface tension. Moreover, the action of the pressure exerted by the CNF walls could also inhibit the phase change, for energy reasons, and maintain the hcp-Co phase.

In order to evaluate the magnetic properties of the cobalt particles obtained by different treatments, magnetic hysteresis measurements were performed in some samples. In Figure 6A, magnetic hysteresis measurements performed on synthesized Co_3O_4 nanoparticles at 5 and 300 K are presented. The $M(H)$ curves are linear with the field and have no coercivity and remenance. The samples cannot reach the saturation even in the presence of 50 kG magnetic field. On the other hand, Figure 6B show the M(H) curves at 5 and 300 K for the sample reduced in H_2+CO atmosphere. In this case, a hysteresis loop is observed and these samples have coercivity (1.1 kG at 5 K and 0.8 kG at 300 K). These results are higher compared with the coercivity measured in fcc-cobalt particles (0.7 kG at 5 K and 0.3 kG) obtained by treatment with H_2 atmospheres, thus showing the beneficial effects of the presence of hcp Co nanoparticles stabilized at high temperatures compared to the non-stabilized fcc phase. However,

(11) (a) Gibbs J. W. In *The Collected Works of J. Willard Gibbs*; Longley, W. R., van Name, R. G., Eds.; Longmans, Green & Co.: New York 1931. (b) Wulff, G. *Z. Kristallogr.* **1901**, *34*, 449.

(12) van Steen, E.; Claeys, M.; Dry, M.E.; van de Loosdrecht, J.; Viljoen, E. L.; Visagie, J. L. *J. Chem. Phys. B* **2005**, *109*, 3575.

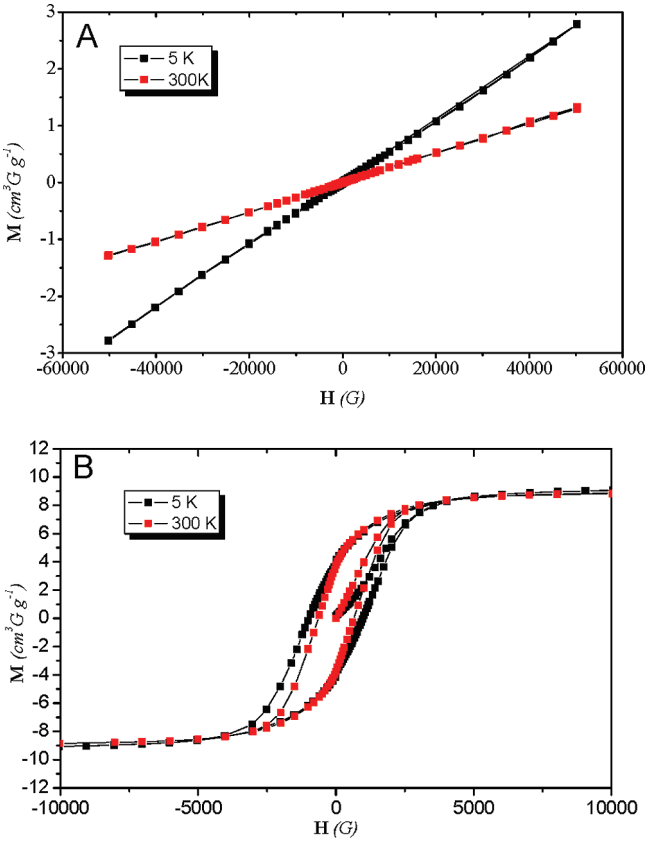

Figure 6. $M(H)$ curve at 5 and 300 K for: (A) Co_3O_4 and (B) Co_3O_4 reduced in a H_2−CO atmosphere at 700 °C.

other factors such as the size and shape of the particles in the sample can dramatically change the coercivity observed.

Conclusion

To conclude, we have observed that the hcp-cobalt metallic phase is produced under H_2+CO atmosphere and is stable at high temperatures (up to 700 °C). This stabilization is due to the encapsulation of cobalt nanoparticles coated by a graphitic layer that leads to the decrease in its surface energy and inhibits the phase change. Moreover, the carbon nanostructures can store unstable cobalt crystalline structures, even at high temperatures, because of the limited mobility of the crystal atoms within an envelope of carbon. Therefore, the carbon coating of hcp-Co particles prevents sintering and avoids the oxidation and tribology process. Besides, this method could be used in the synthesis of cobalt metal particles for magnetic storage or for catalytic applications. These potential applications will be explored in a future paper that will address cobalt−carbon synergism and its additive properties.

Acknowledgment. This work was supported by the Spanish (MAT2005-03456) and Catalan (2005SGR-00184) governments. V.A.P.O. acknowledges financial support from the MCYT in the Juan de la Cierva Program. The assistance of Mr. X. Alcobé and Mr. J. Bassas (SCTUB) with XRD measurements and Nuria Clos with SQUID measurements is gratefully acknowledged.

Supporting Information Available: X-ray powder diffraction patterns, scanning electron microscopy photographs, X-ray photoelectron spectroscopy, transmission electron microscopy photographs, and EELS spectra. This material is available free of charge via the Internet at http://pubs.acs.org.